


RESEARCH

Open Access



Ex vivo expanded human regulatory T cells modify neuroinflammation in a preclinical model of Alzheimer's disease

Alireza Faridar¹, Matthew Vasquez³, Aaron D. Thome¹, Zheng Yin³, Hui Xuan¹, Jing Hong Wang¹, Shixiang Wen¹, Xuping Li², Jason R. Thonhoff¹, Weihua Zhao¹, Hong Zhao³, David R. Beers¹, Stephen T. C. Wong³, Joseph C. Masdeu¹ and Stanley H. Appel^{1*} 

Abstract

Background: Regulatory T cells (Tregs) play a neuroprotective role by suppressing microglia and macrophage-mediated inflammation and modulating adaptive immune reactions. We previously documented that Treg immunomodulatory mechanisms are compromised in Alzheimer's disease (AD). Ex vivo expansion of Tregs restores and amplifies their immunosuppressive functions in vitro. A key question is whether adoptive transfer of ex vivo expanded human Tregs can suppress neuroinflammation and amyloid pathology in a preclinical mouse model.

Methods: An immunodeficient mouse model of AD was generated by backcrossing the 5xFAD onto Rag2 knock-out mice (5xFAD-Rag2KO). Human Tregs were expanded ex vivo for 24 days and administered to 5xFAD-Rag2KO. Changes in amyloid burden, microglia characteristics and reactive astrocytes were evaluated using ELISA and confocal microscopy. NanoString Mouse AD multiplex gene expression analysis was applied to explore the impact of ex vivo expanded Tregs on the neuroinflammation transcriptome.

Results: Elimination of mature B and T lymphocytes and natural killer cells in 5xFAD-Rag2KO mice was associated with upregulation of 95 inflammation genes and amplified number of reactive microglia within the dentate gyrus. Administration of ex vivo expanded Tregs reduced amyloid burden and reactive glial cells in the dentate gyrus and frontal cortex of 5xFAD-Rag2KO mice. Interrogation of inflammation gene expression documented down-regulation of pro-inflammatory cytokines (*IL1A&B, IL6*), complement cascade (*C1qa, C1qb, C1qc, C4a/b*), toll-like receptors (*Tlr3, Tlr4 and Tlr7*) and microglial activations markers (*CD14, Tyrobp, Trem2*) following Treg administration.

Conclusions: Ex vivo expanded Tregs with amplified immunomodulatory function, suppressed neuroinflammation and alleviated AD pathology in vivo. Our results provide preclinical evidences for Treg cell therapy as a potential treatment strategy in AD.

Keywords: Alzheimer's disease, Regulatory T cells, Inflammation, Adaptive immune system, Microglia, Amyloid pathology

Background

The discovery of risk genes involved in inflammation signaling [1–3], indicates that inflammation is critical for the onset and progression of Alzheimer's disease (AD). In AD transgenic mouse models, microglia is one of the initial responders to amyloid- β plaque

*Correspondence: sappel@houstonmethodist.org

¹ Stanley H. Appel Department of Neurology, Houston Methodist Research Institute, 6560 Fannin Street, Suite ST-802, Houston, TX 77030, USA
Full list of author information is available at the end of the article



© The Author(s) 2022. **Open Access** This article is licensed under a Creative Commons Attribution 4.0 International License, which permits use, sharing, adaptation, distribution and reproduction in any medium or format, as long as you give appropriate credit to the original author(s) and the source, provide a link to the Creative Commons licence, and indicate if changes were made. The images or other third party material in this article are included in the article's Creative Commons licence, unless indicated otherwise in a credit line to the material. If material is not included in the article's Creative Commons licence and your intended use is not permitted by statutory regulation or exceeds the permitted use, you will need to obtain permission directly from the copyright holder. To view a copy of this licence, visit <http://creativecommons.org/licenses/by/4.0/>. The Creative Commons Public Domain Dedication waiver (<http://creativecommons.org/publicdomain/zero/1.0/>) applies to the data made available in this article, unless otherwise stated in a credit line to the data.

deposits [4–6]. Activation of microglial pattern recognition toll-like receptors (TLRs) and intracellular NLRP3 inflammasomes induces tau hyperphosphorylation and aggregation [7–11]. Subsequent release of truncated phosphorylated tau also enhances immune cell activation, promoting the release of inflammatory mediators and a self-propagating cascade of synaptic dysfunction, neuronal injury, and cell death [11–14]. The structural integrity of the blood–brain barrier is also impaired in the presence of AD pathology [15–17], thereby permitting substantial crosstalk between the central nervous system (CNS) and peripheral immune system. Thus, circulating immune cells might reflect and contribute to AD pathogenesis [18–20]. Regulatory T cells (Tregs) are a subset of T cells that play a neuroprotective role by suppressing inflammation in the blood and brain [21]. We have previously documented that Treg immunomodulatory mechanisms are compromised in AD patients. As a consequence, there is activation of systemic cytotoxic immune cells and upregulation of pro-inflammatory mediators [22]. Accumulating preclinical and clinical evidences suggest Tregs as a modifiable therapeutic target. Ex vivo expansion of dysfunctional Tregs in AD individuals not only restored but enhanced their immunosuppressive function [22]. Restoration of Tregs is currently being translated into cell therapy for neurodegenerative disorders. Recently, our group has conducted a first-in-human Phase I trial of expanded autologous Treg infusions in Amyotrophic Lateral Sclerosis (ALS) [23]. The study demonstrated safety and potential benefit of this treatment strategy, and a Phase II double blind, placebo-controlled study is currently underway. The promising therapeutic potential of autologous infusions of expanded Tregs in ALS raised the question as to whether a similar strategy would be of value in AD. In the current study, we investigated the impact of ex vivo expanded human Tregs on neuroinflammation and A β pathogenesis in a preclinical AD system.

The widely used 5xFAD mice model recapitulates early and aggressive features of AD pathology with sustained microglial activation, increased inflammation markers and abundant deposition of plaques at early ages [24, 25]. To evaluate the role of the adaptive immune system on AD pathology, a mouse model of AD was generated by backcrossing the 5xFAD mouse onto a Rag2 Il2ry^{-/-} double knockout mice (5xFAD-Rag2KO). The resulting mice lack T cells, B cells and natural killer (NK) cells. This Rag2KO mouse model is an appropriate host for xenogeneic human cell engraftment with minimal host versus graft reaction [26–31]. Ex vivo expanded human Tregs with remarkably enhanced immunosuppressive function were adoptively transferred to the immunodeficient

5xFAD-Rag2KO mice. Following peripheral administration, Tregs were detectable in the frontal cortex and dentate gyrus. They effectively reduced numbers of reactive microglia and astrocytes, suppressed neuroinflammation transcriptome and alleviated amyloid burden.

Methods

Generation of a Rag2 Il2ry^{-/-} knock out immune-deficient AD mouse model

All animal protocols were approved by the Methodist Research Institute's Institutional Animal Care and Use Committee in compliance with National Institutes of Health guidelines. Rag2 Il2ry^{-/-} double knock out mice were initially bred with purebred 5xFAD and strain-matched wild-type C57BL/6 mice to generate immune-deficient 5xFAD-Rag2KO and strain-matched WT-Rag2KO mice. The presence or absence of the Rag2 gene was determined by PCR using 250 ng of tail DNA and Eppendorf TaqDNA polymerase according to the manufacturer's instructions. The following primers were used: Rag A) 5'-GGGAGGACACTCACTTGC-CAG-3' and Rag B) 5'-AGTCAGGAGTCTCCATCTCAC-3' and Neo C) 5'-CGGCGG-GAGAACCCTGCGTGCAA-3'. Homozygotic mice will have one 350 bp band. Heterozygotic mice will have 350 and 263 bp bands. Wild-type mice will have one 263 bp band. Therefore, six groups of mice were characterized in this study including WT-5xFAD, 5xFAD-Rag2KO, Treg-treated 5xFAD-Rag2KO, WT-WT, WT-Rag2KO and Treg-treated WT-Rag2KO mice. There were total 10 mice per group, sex balanced (5 female & 5 male).

Ex vivo expansion of human Tregs and passive transfer to mice

Human CD4⁺CD25^{high} T lymphocytes were isolated from peripheral blood of a healthy subject using the Regulatory T Cell Isolation Kit (Miltenyi Biotec) according to the manufacturer's instructions. Tregs were suspended at a concentration of 1×10^6 cells/ml in media containing 100 nM of rapamycin (Miltenyi Biotec), 500 IU/ml IL-2 (Miltenyi Biotec) and DynabeadsTM Human Treg Expander (GibcoTM) at a 4:1 bead-to-cell ratio for 8 days (First stimulation). At day 8, beads were removed, and cells were resuspended in a culture medium containing 100 U/mL IL-2 and 100 nM of rapamycin for 8 days. On day 16, Tregs were restimulated by adding Dynabeads expansion beads at a 1:1 bead-to-cell ratio for further 8 days. After the second stimulation, Tregs were harvested and washed on day 24. The Treg immunophenotype and suppressive function were assayed prior to injection to mice, as described previously [22]. Based on the data obtained from similar studies in infusing Treg

into preclinical mice model [32–34], and considering temporal expression profile of CNS inflammatory genes in 5xFAD mice [24], the current study was designed to administer 1×10^6 ex vivo expanded Tregs, suspended in a 200 μ l of phosphate-buffered saline (PBS), into 5-month-old 5xFAD-Rag2KO and WT-Rag2KO mice via tail vein injections. This treatment was repeated every month for a total of 5 months and the mice were sacrificed at age 10 months.

RNA sample preparation and transcriptome analysis

Using Trizol reagent, followed by Direct-zol RNA Mini-Prep Kit (Zymo Research), messenger RNA was extracted from medial temporal cortex and frontal cortex of mice. For mouse neuroinflammation panel analysis, 770 transcripts were quantified with the NanoString nCounter multiplexed target platform (www.nanostring.com). nCounts of mRNA transcripts were normalized using the geometric means of 10 housekeeping genes (Csnk2a2, Ccdc127, Xpnpep1, Lars, Supt7l, Tada2b, Aars, Mto1, Tbp, and Fam104a).

Protein extraction and ELISA assay

The right hemisphere samples were homogenized in a 2% SDS lysis buffer (SDS, NaCl 150 mM and Triton™ 1%) containing phosphatase (Pierce) and protease (Roche) inhibitors. After centrifugation (60 min, 100,000 \times g, 4 °C), the supernatant was collected (SDS extract) and the protein concentration was quantified. 70% formic acid in water was added to the pellet and the supernatant was collected after sonication and centrifugation (FA extract). Soluble (SDS extract) and insoluble (FA extract) A β 40 and A β 42 were measured using Amyloid beta Human ELISA Kit (Invitrogen).

Immunofluorescence staining

Splenocytes were isolated from spleens for flow cytometric analysis. Antibodies against the following surface markers were provided by: CD3 FITC (eBioscience™), CD4 PE (eBioscience™), CD8a Alexa Fluor 700 (eBioscience™), CD161 APC (eBioscience™) and CD19 PE-Cy5 (eBioscience™). Dead cells were stained by LIVE/DEAD® Fixable Blue Dead Cell Stain Kit (Life Technology). For immunohistochemical brain analyses, the left cerebral hemisphere was dissected and post-fixed in 4% paraformaldehyde in 0.1 M PBS for 2 days. Brains were cryoprotected by incubation in a 30% sucrose/0.1 M PBS solution. Sagittal brain sections were cut on a freezing microtome (Leica) and collected serially. Immunohistochemistry was performed on free-floating microtome-cut Sects. (10 μ m in thickness). Sections were incubated with different antibodies:

anti-mouse Iba1 (Polyclonal, 1:1000 Wako), anti-mouse CD68 (Clone FA-11, 1:200; BioRad), β -Amyloid (Clone 6E10, 1:1000; BioLegend), β -Amyloid 1–42 (polyclonal, 1:100; Millipore), anti-mouse GFAP (Clone GA-5, 1:100, Novus Biological) anti-human CD3 (Clone: CD3-12, 1:100, abcam) and anti-human Foxp3 (Clone 236A/E7, 1:100, Invitrogen). Appropriate secondary antibodies (Alexa Fluor 488, 594, or 647; Invitrogen) were used followed by incubation with DAPI.

Confocal image quantification

After immunofluorescence staining, 2D single plane image were captured using a Nikon A1 laser scanning confocal microscope. The system uses a galvanometer scanner with a 20 \times Plan Apo objective, and a pinhole set to 1.2 Airy Unit. Laser power, numeric gain and magnification were kept constant between animals to avoid potential technical artefacts. NIS Elements Version 5.11.01 was used to quantify mean intensity of fluorescence, number of immunoreactive cells, and size of plaques. The region of interest to analyze was done across the field of view of the whole image acquired. Since each image was 1024 \times 1024 pixels with a resolution at 0.63 μ m/pixel, we measured the amount of immunoreactive cells in a 416,179.81 μ m² area of frontal cortex or dentate gyrus. All absolute quantifications were performed at \times 20 magnification. The DAPI mask of detected nuclei was used as a reference to generate the count of positive microglial cells. Any mask of detected microglial signal that had overlapping signal with the DAPI mask of detected nuclei were considered positive microglial cells and a new detected objects mask was created. All other detected DAPI nuclei were excluded from this new mask. In evaluating number of microglia that were surrounding plaques (within 20- μ m radius of the 6E10-positive plaques), two separate FITC masks of detected amyloid beta plaques were generated. One mask of detected amyloid beta plaques was used to gain an accurate measurement of amyloid beta plaque area and count. The other mask of detected amyloid beta plaques was a copy of the first amyloid beta plaque mask but with the implementation of dilating the mask to increase the diameter up to an additional 20 μ m. The new DAPI nuclei mask of positive microglial cells, mentioned earlier, was used to determine the quantity of microglial cells associated with the dilated mask of detected amyloid beta plaques by overlaying both masks. After analysis of the masks of detected objects, statistical data was retrieved. The counts of positive glial cells, count of positive glial cells associated with amyloid beta plaques, the total detected area

of amyloid beta plaque, the summation of all detected amyloid beta plaque signal intensity, and total count of detected amyloid beta plaque were analyzed.

Statistical analysis

In this exploratory study, we applied resource equation method with projected attrition of 20, to determine the sample size in each group, as described previously [35, 36]. All experiments in this study were blinded and randomized by blocks of animals. The experimental design and handling of mice were identical across experiments. The vehicle group were treated with the same volume of vehicle via tail vein injections. The analyses, including immunohistochemistry staining, ELISA and transcriptome analysis were performed by blinded independent investigators. Statistical analysis was performed using Prism 7.0 (GraphPad Software). The significance of group comparisons was tested using paired or unpaired student's t-test (for two groups) or one-way ANOVA (for more than two groups). Data were expressed as Mean \pm SEM and p values less than 0.05 were considered significant. For transcriptome analysis, nSolver software was used for background subtraction and normalization of data. Statistical analysis on the normalized expression profiles, including one-way ANOVA and multiple comparison using Tukey's range test, were carried out using the Statistics and Machine Learning Toolbox in MATLAB R2020a. Volcano plots of differential expressed genes data were plotted using GraphPad Prism. Gene enrichment analysis was performed using Ingenuity pathway analysis (IPA).

Results

Treg administration alleviates amyloid burden in immunodeficient AD mice

We generated 5xFAD-Rag2KO and WT-Rag2KO mice by backcrossing the 5xFAD and C57BL/6 J mice onto a Rag2 Il2ry^{-/-} double knock out background. We have documented lack of adaptive immune system including CD4 and CD8 T cells, B cells and NK cells in transgenic

Rag2KO mice (Additional file 1: Fig. S1A). These cells are the key immune components involved in xenogeneic cell rejection. Strain-matched immunocompetent AD and wild-type (WT) mice, termed 5xFAD-WT and WT-WT respectively, were also developed. CD4⁺CD25^{high}Tregs were isolated from peripheral blood of a healthy human subject and expanded ex vivo. After two rounds of stimulation, the number of Tregs was increased 56 times within 24 days (Additional file 1: Fig. S1B). The increase in number of Tregs following ex vivo expansion, was associated with amplification in mean fluorescence intensities (MFI) of immunomodulatory markers including Foxp3, CD25, PD1 and CD73 (Additional file 1: Fig. S1C–F). We also evaluated the immunosuppressive function of Tregs at baseline and following 8 and 24 days of ex vivo expansion. The suppressive function of Treg on corresponding CD4⁺CD25⁻ T responder (Tresp) proliferation and iPSC-derived pro-inflammatory myeloid cells (M1) cytokine expressions were significantly enhanced following ex vivo expansion (Additional file 1: Fig. S1G–J). Tregs vs. vehicle were adoptively transferred into 5xFAD-Rag2KO and WT-Rag2KO mice and the presence of Tregs in the murine brain was evaluated after 2 weeks with co-labeling against CD3 and Foxp3 as described previously [32]. Human Tregs were detected and quantified in the DG and FC of 5xFAD-Rag2KO mice following peripheral administration, suggesting that these human cells survived in immunocompromised mice and distributed into the CNS (Fig. 1J–L, Additional file 1: Fig. S2).

Highly sensitive multiplex ELISA was performed to quantify the burden of SDS-soluble and formic acid (FA) treated insoluble A β within the brains of immunocompetent 5xFAD-WT, immunodeficient 5xFAD-Rag2KO and Treg-treated 5xFAD-Rag2KO mice (n = 10/group; sex-balanced). In the absence of the adaptive immune system, there was a trend toward increased levels of A β 40 and A β 42 species in 5xFAD-Rag2KO, compared to 5xFAD-WT. Treg administration effectively reduced the levels of both soluble and insoluble A β 40 and A β 42 in 5xFAD-Rag2KO mice, compared to the untreated group. Levels

(See figure on next page.)

Fig. 1 Treg treatment suppress Amyloid pathology. **A** ELISA quantification of mice brain homogenates shows a trend toward an increased levels of SDS-soluble and formic acid treated insoluble A β 40 and A β 42 in 5xFAD-Rag2KO, compared to 5xFAD-WT. Ex vivo expanded Treg administration decreased both soluble and insoluble A β 40 and A β 42 burden in 5xFAD-Rag2KO (10-month-old mice, 10 per group; sex-balanced). **B, C** Representative images of A β immunostaining (6E10) of the dentate gyrus (DG) and frontal cortex (FC) in 5xFAD-WT, 5xFAD-Rag2KO and Treg-treated 5xFAD-Rag2KO. **D–I** Quantification of the 6E10-positive amyloid aggregates in the DG and FC. The percentage of area covered by A β in the DG were increased in 5xFAD-Rag2KO compared to 5xFAD-WT. Number of plaques and their signal intensity were comparable between 5xFAD-Rag2KO and 5xFAD-WT in both DG and FC. Ex vivo expanded Treg administration reduced area covered by plaque, number of plaques and their signal intensity in both DG and FC of 5xFAD-Rag2KO mice (n = 6–7 per group). **J** Immunostaining of Tregs (CD3 in red, Foxp3 in green) and cell nuclei (DAPI in blue) in the DG of 10-month-old 5xFAD-Rag2KO mice treated with human Tregs or Phosphate-buffered saline (PBS). **K, L** Quantification of number of CD3⁺Foxp3⁺ Tregs in the DG and FC of 4 groups of mice including Treg treated 5xFAD-Rag2KO, Treg treated WT-Rag2KO, PBS treated 5xFAD-Rag2KO and also PBS treated WT-Rag2KO mice. Numbers shown as averages \pm SEM with one-way ANOVA. P-values are *p < 0.05, **p < 0.01, ***p < 0.001, ****p < 0.0001. Scale bar, 100 μ m

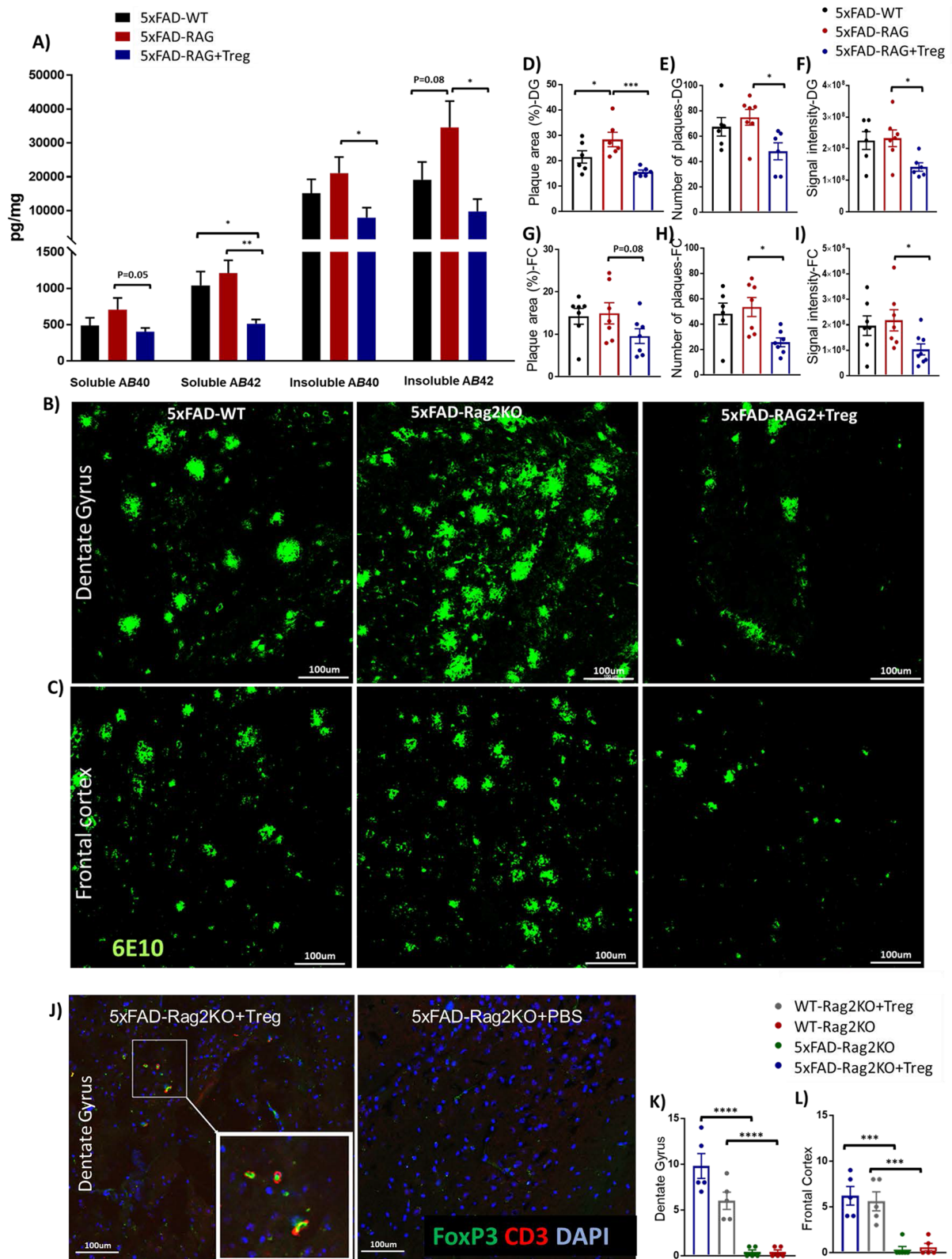


Fig. 1 (See legend on previous page.)

of soluble A β 42 in Treg-treated 5xFAD-Rag2KO were even lower than in the immunocompetent 5xFAD-WT group (Fig. 1A). Soluble and insoluble A β 40 and A β 42 were undetectable in WT-WT and WT-Rag2ko mice. Sections of dentate gyrus (DG) and frontal cortex (FC) were also immunolabeled with 6E10 antibody to assess plaque load, using confocal microscopy (Fig. 1B, C). As expected, 5xFAD-WT mice, at age 10-month, showed highly abundant plaques in the DG and FC. In comparison between 5xFAD-WT and 5xFAD-Rag2KO, while the number of plaques (Fig. 1E, H) and their signal intensities (Fig. 1F, I) were comparable, the absence of T, B and NK cells in 5xFAD-Rag2KO, further increased the percentage of area covered by A β in the DG (Fig. 1D). Following Treg administration, the total plaque area (Fig. 1D, G) and the number of plaques (Fig. 1E, H) within the DG and FC of 5xFAD-Rag2KO mice were alleviated. The signal intensity of plaques was also lowered in the Treg-treated AD group, suggesting reduced plaque compaction following Treg administration (Fig. 1F, I).

Treg administration modifies glial cells in AD mice

Compared to WT, the 10-month-old 5xFAD-WT mice showed 2–3 folds increases in the number of Iba1⁺ microglia in the DG and the FC. The total number of Iba1⁺ microglia was comparable between 5xFAD-WT and 5xFAD-Rag2KO and remained unaltered after Treg administration (Fig. 2A, B, Additional file 1: Fig. S3A, B). In evaluating number of microglia that were surrounding plaques (within 20- μ m radius of the 6E10-positive plaques), there was a trend toward increased level of plaque associated Iba1⁺ microglia in the DG of 5xFAD-Rag2KO mice, compared to 5xFAD-WT (Fig. 2C). Treg administration significantly reduced plaque associated Iba1⁺ microglia in the DG (Fig. 2C). In the next step, the number of activated microglia was assayed in the DG and FC, using CD68 staining (Fig. 2D and Additional file 1: Fig. S3D). The number of CD68⁺ microglia within the DG was increased following elimination of T, B and NK cells in 5xFAD-Rag2KO mice, compared to 5xFAD-WT (Fig. 2E). Treg treatment significantly reduced total and plaque associated CD68⁺ microglia in both DG (Fig. 2E,

F) and FC of 5xFAD-Rag2KO (Additional file 1: Fig. S3E, F).

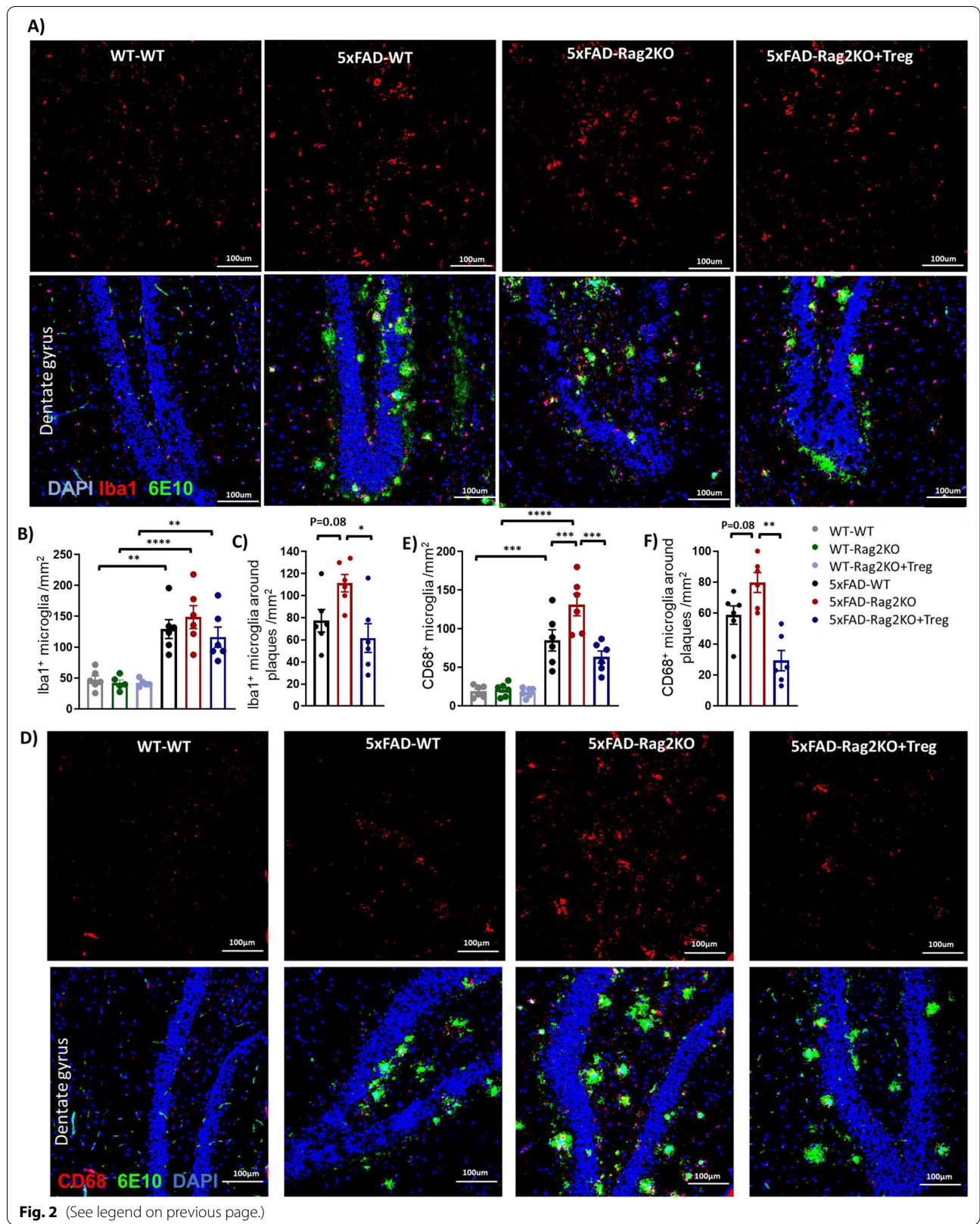
In the next step, reactive astrocytes were evaluated in the DG and FC, using GFAP staining. There were major differences in astrocyte state in AD relative to WT group, as number of GFAP⁺ reactive astrocytes in 5xFAD mice were about 4 folds higher than WT mice in the DG and FC (Fig. 3A, F). While number of GFAP⁺ reactive astrocytes were comparable between 5xFAD-WT and 5xFAD-Rag2 KO group, Treg treatment significantly alleviated number of GFAP⁺ reactive astrocytes in both DG and FC of 5xFAD-Rag2 KO mice (Fig. 3B, D). In evaluating plaque associated reactive astrocytes, there was a trend toward increased level of GFAP⁺ reactive astrocytes that were located within 50 μ m of amyloid plaques in the DG and FC of 5xFAD-Rag2KO mice compared to 5xFAD-WT. Treg treatment suppressed plaque associated GFAP⁺ reactive astrocytes in both DG and FC (Fig. 3C, E).

Identification of differentially expressed inflammation genes following adaptive immune system modification

NanoString gene expression panel of 770 mouse immune factors was applied in the extracted RNA from the hippocampus of WT-WT, WT-Rag2KO, 5xFAD-WT, 5xFAD-Rag2KO and Treg-treated 5xFAD-Rag2KO. Comparing of 5xFAD-WT with WT-WT mice, 73 immune related genes were upregulated (Fold change (FC) >1.5, $p < 0.05$) and only 4 genes were downregulated (FC < 0.66, $p < 0.05$) in AD mice (Fig. 4A). Genes implicated in microglial/macrophage activation [*Clec7a*: FC = 14.7, *Ccl3*: FC = 11.7, *Cst7*: FC = 9.0, *Trem2*: FC = 5.4, *Tyrobp*: FC = 4.36, *Cd68*: FC = 3.6] as well as complement activation (*Itgax*: FC = 5.5, *C4a*: FC = 4.2) were most highly upregulated in 10-month-old 5xFAD-WT mice (Fig. 4A), supporting the role of neuroinflammation in AD pathogenesis. Comparing 5xFAD-Rag2KO with WT-Rag2KO, 95 immune genes were upregulated and 7 genes were down-regulated in immunocompromised AD mice. Lack of T, B and NK cells in 5xFAD-Rag2KO further strengthened the pathological overexpression of microglial/macrophage (*Clec7a*: FC = 19.0, *Cst7*: FC = 14.6, *CCL3*: FC = 11.3, *Trem2*: FC = 8.0, *Tyrobp*: FC = 7.0 and *CD68*:

(See figure on next page.)

Fig. 2 Treg administration reduces number of activated microglia in the dentate gyrus. **A** Representative images of Iba1 positive-microglia (red) and 6E10-positive A β plaques (green) in the dentate gyrus (DG) of WT-WT, 5xFAD-WT, 5xFAD-Rag2KO and Treg-treated 5xFAD-Rag2KO (n = 6 per group, sex balanced). **B** Quantification of the number of Iba1⁺ microglia in the DG; while number of Iba1⁺ microglia was increased in 5xFAD-WT mice, compared to WT-WT, lack of adaptive immune system in 5xFAD-Rag2KO and subsequent Treg administration had no effect on the number of Iba1⁺ microglia. **C** Quantification of the number of Iba1⁺ microglia within 20 μ m of the plaque surface; Treg administration reduced number of plaque-associated Iba1⁺ microglia. **D** Representative images of CD68-positive activated microglia (red) and 6E10-positive A β plaques (green) in the dentate gyrus. Quantification of CD68-positive activated microglia in the DG (**E**) and CD68-positive microglia within 20 μ m of the plaque surface (**F**), revealed decreased number of total and plaque-associated CD68⁺ microglia in 5xFAD-Rag2KO following Treg administration. Numbers shown as averages \pm SEM with one-way ANOVA. * $p < 0.05$, ** $p < 0.01$, *** $p < 0.001$ and **** $p < 0.0001$. Scale bar, 100 μ m



FC=6.1) and complement activation (*Itgax*: FC=8.1, *C4a*: FC=6.2) markers (Fig. 4B). Finally, we evaluated the impact of ex vivo expanded human Tregs on modulating neuroinflammation transcriptome. 71 out of 99 upregulated genes in 5xFAD-Rag2KO, had opposite direction of fold changes following Treg treatment, which suggests Treg treatment is pulling the expression profile of these immune genes away from 5xFAD-Rag2KO and towards WT-Rag2KO (Fig. 4C). Applying Ingenuity's pathway analysis, we interrogated these genes with respect to enriched network and subcellular compartments. The enriched network was centered in extracellular complements activation (*C1qa*, *C1qb*, *C1qc*, *C4a/b*), pro-inflammatory cytokine networks (*IL1A&B*, *IL6*, *Tnfa*, *Ifny*), membrane binding receptors of toll like receptors (*Tlr3*, *Tlr4* and *Tlr7*) and myeloid activation markers (*Cd14*, *Tyrobp*, *Trem2*, *Cd68*). In addition, nuclear localized binding motifs of the interferon-regulatory factors (*Irf3* and *Irf7*) which provides further evidence for modification of interferon response-related genes following Treg treatment (Fig. 4D). In order to evaluate the finding of pathway integrative analysis beyond the hippocampus, 10 enriched genes in hippocampal analysis, including complement activation markers (*C1qa*, *C1qb*, *C1qc*), pro-inflammatory cytokines (*IL1B*, *IL6*, *TNFa*), microglial activation markers (*Tyrobp*, *Trem2*) and transmembrane protein genes of *Tlr3* and *Itgax* were analyzed in the extracted RNA from the frontal cortex, using quantitative real-time PCR. 8 out of 10 selected genes were significantly upregulated in 5xFAD-RAG2 KO mice, and subsequently down-regulated or had a trend toward reduced expressions following Treg administration (Additional file 1: Fig. S4).

Discussion

Our study characterized the impact of ex vivo expanded human Tregs in a preclinical AD model. Following peripheral administration, Tregs were detectable in the central nervous system of immunodeficient AD mice and reduced reactive glial cells and amyloid burden. Similar to our finding, systemic Treg expansion in transgenic AD mice models, including low dose IL-2 administration, modified neuroinflammation and enhanced neuroprotection against AD pathology [32, 37, 38]. However, Tregs might have dichotomous effects on the

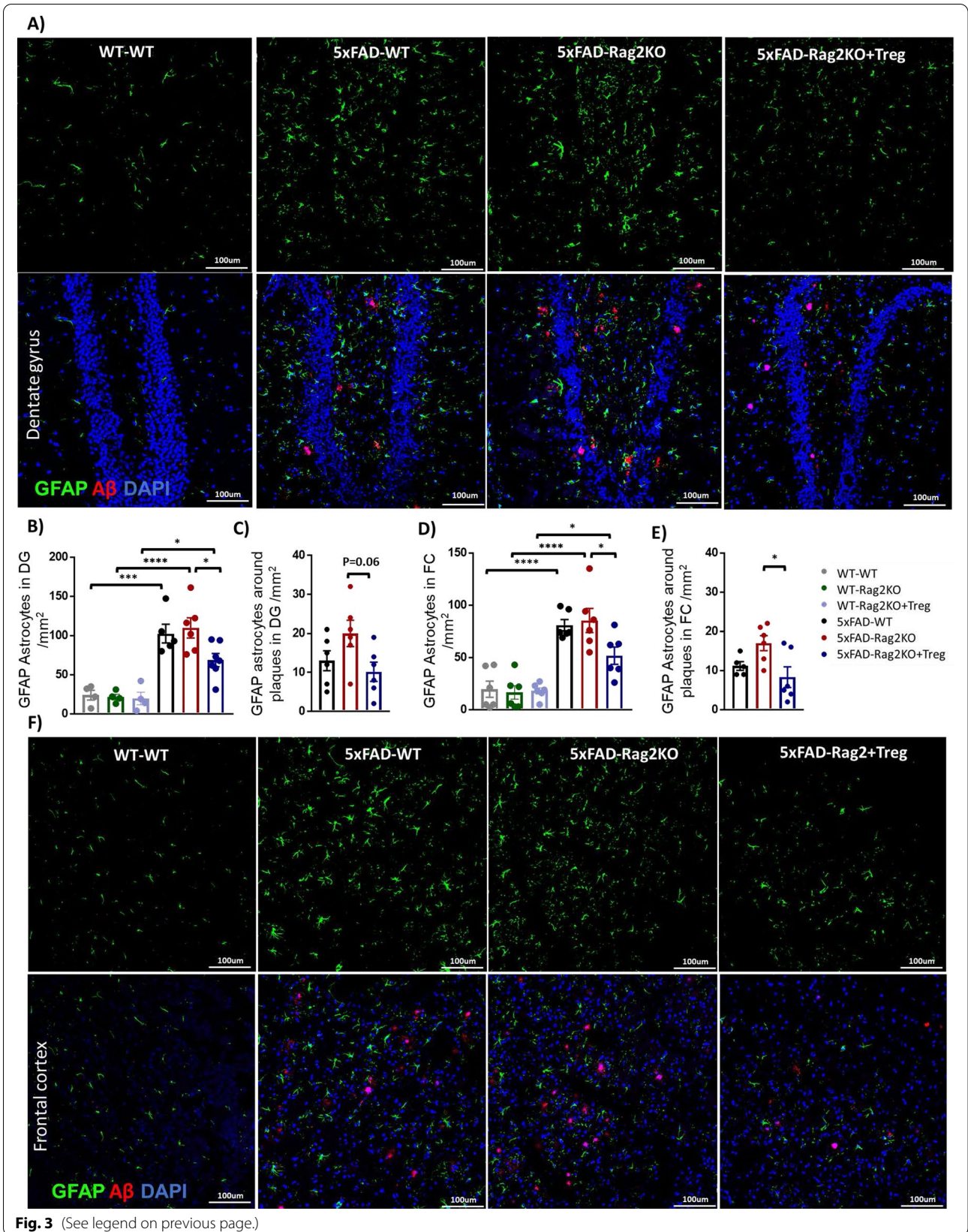
neurodegenerative process by obstructing a selective gateway for immune cell trafficking to the CNS, reducing the recruitment of immunoregulatory cells from the periphery to the CNS particularly in juvenile mice [39]. We believe that in older AD mice, in the presence of AD pathology, or in the clinical setting of Alzheimer's disease, the structural integrity of the blood–brain barrier has already broken down and peripheral immune cells would migrate through the activated endothelium by various mechanisms.

We initially generated immunocompromised AD mice model with lack of adaptive immune system. Genetic ablation of T cells, B cells and NK cells in AD mice, further amplified the expression of pathologic inflammatory genes involved in complement cascade and microglial activation. The activation of complement cascade and pro-inflammatory microglia can lead to synaptic dysfunction, neuronal death and inhibition of neurogenesis [40–42]. The upregulation of these neuroinflammatory networks and increased number of activated glial cells in this study were associated with increased percentage of area covered by A β , as reported previously [43]. In contrast to our finding and Marsh et al. study that applied Rag2 *Il2ry*^{-/-} double knock out in 5xFAD mice (Lack of B, T and NKC), Späni et al. used single knock out Rag2 PSAPP transgenic mice (NKC sufficient) with contradicting reduction in CNS amyloid burden [44]. Together, these results indicate that NK cells might play a considerable role in microglial activation and amyloid pathology.

Accumulating preclinical and clinical evidences suggest that adaptive transfer of ex vivo expanded Tregs is a novel therapeutic strategy to modulate chronic inflammation in neurodegenerative processes [23]. Following ex vivo expansion, the immunophenotype and suppressive function of ex vivo expanded Tregs were substantially restored and amplified. In the current study, we investigated the modulatory effect of ex vivo expanded human Treg with amplified immunosuppressive function on AD pathology in a preclinical AD mice model. The 5xFAD-Rag2KO mice lack T cells, B cells and natural killer cells, key immune components involved in xenogeneic cell rejection and are suitable for engraftment of human cells without preconditioning [26–31, 45–47]. Following peripheral administration, Tregs were detectable in the dentate gyrus and frontal cortex of mice. This

(See figure on next page.)

Fig. 3 Treg administration reduces number of reactive astrocytes. Representative images of GFAP positive-reactive astrocytes (green) and A β 1–42 positive plaques (red) in the dentate gyrus (DG) (A) and frontal cortex (FC) (F) of WT-WT, 5xFAD-WT, 5xFAD-Rag2KO and Treg-treated 5xFAD-Rag2KO (n = 6 per group, sex balanced). B–E Quantification of the number of GFAP⁺ reactive astrocytes in the DG and FC; number of GFAP⁺ reactive astrocytes was increased in 5xFAD-WT mice, compared to WT-WT. Lack of adaptive immune system in 5xFAD-Rag2KO had no effect on the number of GFAP⁺ reactive astrocytes, compared to 5xFAD-WT. Decreased number of total and plaque-associated GFAP⁺ reactive astrocytes in 5xFAD-Rag2KO were noted following Treg administration. Numbers shown as averages \pm SEM with one-way ANOVA. **p* < 0.05, ***p* < 0.01, ****p* < 0.001 and *****p* < 0.0001. Scale bar, 100 μ m



finding is consistent with previous study that has shown survival of human Treg in immunocompromised mice for at least 40 days after administration [33] and also supported transmigration of peripheral Tregs into the CNS [38, 48, 49]. To monitor immunophenotypic persistence of adoptively transferred Tregs in vivo, in a separate experiment, we isolated lymphocytes from the blood and spleen, 3 and 7 days following peripheral infusion of human Tregs, to reevaluate their characteristics with flow cytometry. However, the number of events appeared to be very low with unreliable immunophenotypic analysis (unpublished data). In this regard, further studies are still required to assess the detailed distribution and immunophenotypic persistence of adoptively transferred Treg following peripheral administration. Other potential limitations in interpretation of our finding is the unknown specificity of human Tregs on modifying neuroinflammation rather than nonspecific effect of human cells in a preclinical AD mice model and also unknown extend of cross-reactivity between human Tregs immunomodulatory markers and mice immune system, as the presence of mice MHC rather than human MHC might limit the function of human Treg. However, the amplified expression of immunomodulatory markers including CTLA4, CD73 and PD1 on the surface of polyclonally expanded Treg cell clearly can contribute to the suppressive mechanism of action and modulating glial cells that is independent of HLA expression.

Microglia are one of the initial responders to amyloid- β plaque deposits [4–6]. While, low concentrations of A β can be taken up by microglia and concentrated into acidic vesicles. Excessive accumulation of A β within microglial lysosomes might induce cellular death, potentially contributing to plaque expansion through the release of A β aggregates at the site of microglial death [50]. In this context, other studies identified roles of activated inflammatory microglia in initiating and expanding plaque pathogenesis rather than phagocytosis and removal [50–53]. In our study, Treg administration to 5xFAD-Rag2KO mice, did not alter overall microgliosis but did reduce the number of reactivate microglia surrounding the plaques.

Astroglia are thought to be the most prevalent cell type in the brain [54, 55]. A β oligomers and inflammatory mediators transform resting astrocytes to hyperplastic and hypertrophic GFAP-high disease associated astrocytes which secrete further pro-inflammatory cytokines and upregulate APP expression [56–58]. In a recent study, adaptive transfer of Tregs into Rag2KO mice suppressed neurotoxic astrogliosis in the chronic phase of stroke [59]. Our data expands this finding to AD pathology as Treg therapy effectively alleviated total and plaque associated GFAP⁺ reactive astrocytes in both dentate gyrus and frontal cortex.

Finally, the pathologic upregulation of inflammation genes in 5xFAD-Rag2KO was modified following Treg administration. Using Ingenuity Pathway Analysis, we noted that the enriched pathways were mainly associated with down-regulation of pro-inflammatory cytokines (*IL1A&B*, *IL6*), complement cascade (*C1qa*, *C1qb*, *C4a/b*), toll like receptors (*Tlr3*, *Tlr4* and *Tlr7*) and microglial activations markers (*CD14*, *Tyrobp*, *Trem2*). These canonical signaling pathways are mainly reported as part of “microglial pro-inflammatory responses” to toxic A β [60]. We propose that reduced number of plaque-associated glial cells and suppression of pro-inflammatory signaling pathways within these cells following Treg therapy have attenuated the contribution of these toxic glial cells in AD pathology and mitigated amyloid burden. However, further investigation is required to evaluate Treg potential effects on AD glial heterogeneity and single cell immunophenotypic shifting.

Conclusion

In this study, ex vivo expanded human Tregs were adoptively transferred to immunodeficient 5xFAD-Rag2KO mice. Following peripheral administration, Tregs were detectable in the central nervous system, suppressed neuroinflammation and substantially alleviated amyloid pathogenesis. These promising preclinical findings provide a rationale for enhancing Treg immunomodulatory function with infusions of ex vivo expanded Tregs or in vivo expansion of endogenous Tregs in patients with Alzheimer’s disease.

(See figure on next page.)

Fig. 4 Modification of inflammation network following Treg administration. Volcano Plots showing fold changes vs. p-values of nCounter Mouse Neuroinflammation panel in **A** 5xFAD-WT vs. WT-WT; 73 immune related genes were upregulated (green dots) and 5 genes were down regulated (blue dots) in 5xFAD-WT (n = 4 in each groups). **B** Compared with WT-Rag2KO, 95 genes were upregulated (green dots) and 7 genes were down-regulated (blue dots) in 5xFAD-Rag2KO. The 10 most upregulated genes and all down-regulated genes are labeled in the figures. **C** Treg-treated 5xFAD-Rag2KO vs. 5xFAD-Rag2KO; the pathologic upregulation of inflammation related genes in 5xFAD-Rag2KO were modified following Treg administration. **D** The network representation and subcellular assignment of the enriched pathway in Treg-treated 5xFAD-Rag2KO vs. untreated 5xFAD-Rag2KO. The enriched network were centered in down-regulation of pro-inflammatory cytokines (*IL1A&B*, *IL6*, *Tnfa*, *IFN γ*), complement activation (*C1qa*, *C1qb*, *C1qc*, *C4a/b*), toll like receptors (*Tlr3*, *Tlr4* and *Tlr7*), myeloid activation markers (*CD14*, *Tyrobp*, *Trem2*) and intra-nuclear binding motifs of interferon-regulatory factors (*IRF3* and *IRF7*)

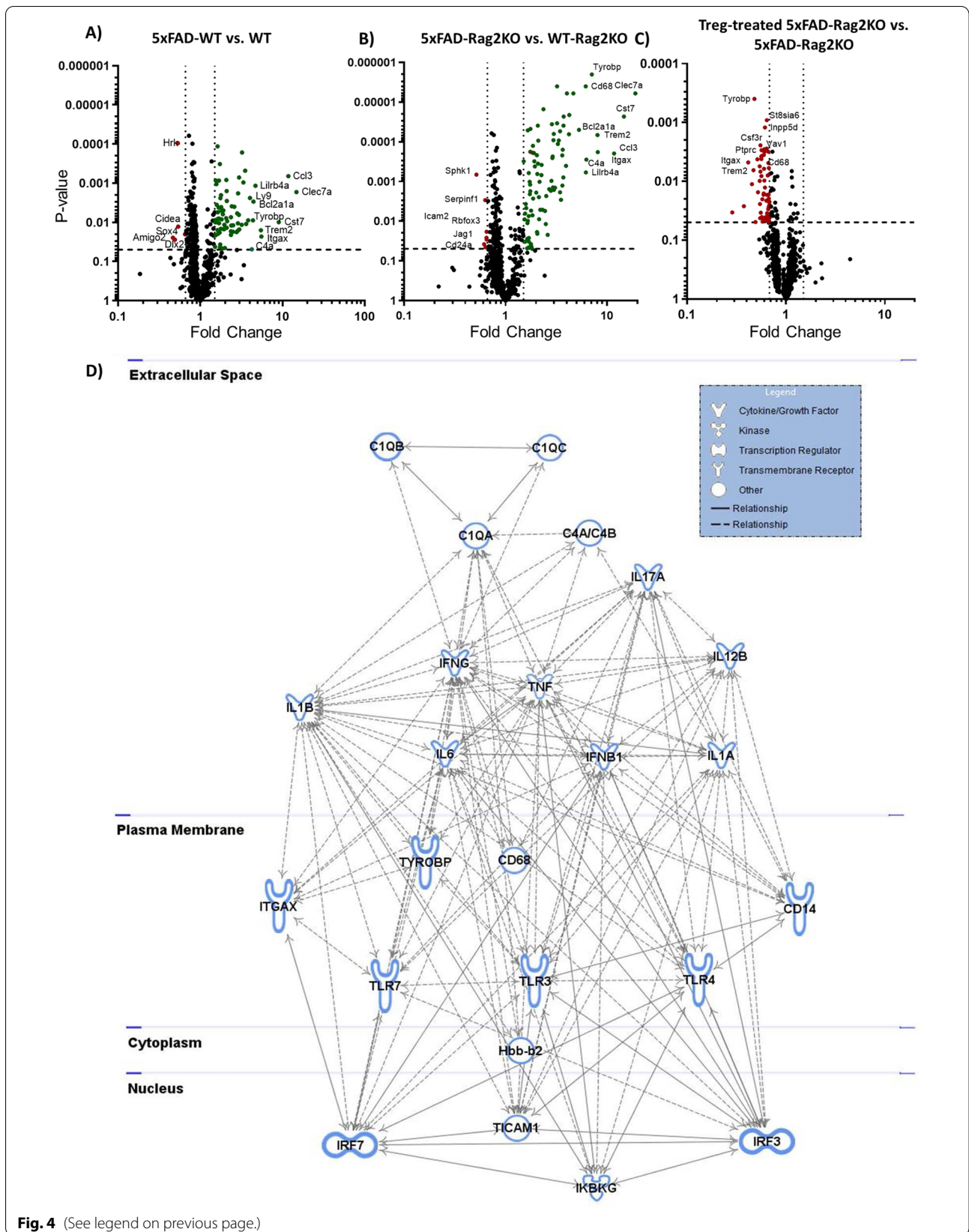


Fig. 4 (See legend on previous page.)

Abbreviations

AD: Alzheimer's disease; ALS: Amyotrophic lateral sclerosis; CNS: Central nervous system; FA: Formic acid; FC: Fold change; IPA: Ingenuity pathway analysis; iPCS: Induced pluripotent stem cells; MFI: Mean Fluorescence Intensities; NK: Natural killer; Treg: Regulatory T cells; Tresp: T responders; TLR: Toll-like receptors; WT: Wild type.

Supplementary Information

The online version contains supplementary material available at <https://doi.org/10.1186/s40478-022-01447-z>.

Additional file 1. Supplementary Figure 1: Characteristics of ex vivo expanded Tregs. Supplementary Figure 2: The presence of Tregs in the frontal cortex following peripheral administration. Supplementary Figure 4: Inflammation gene expressions in the frontal cortex.

Acknowledgements

Acknowledgement is made to the donors of Alzheimer's Disease Research, a program of the BrightFocus Foundation. We are grateful to the Nantz National Alzheimer Center donors for making this research possible. We want to thank Houston Methodist Research Institute's Advanced Cellular and Tissue Microscopy Core Facility for the support.

Author contributions

AF, JCM and SHA conceived and designed research; AF, ADT, HX, JHW, XL, SW, JRT, WZ, DRB performed 5xFAD-Rag2 studies; AF, MV and HZ performed confocal microscopy analysis. Computational analysis of the RNA-seq data was performed at gene expression level by AF, ZY and STW. AF wrote manuscript with input from all authors. All authors read and approved the final version of the manuscript.

Funding

This research was supported by a BrightFocus foundation fellowship award and an award from the Houston Methodist Clinician Scientist Recruitment and Retention Program.

Availability data and material

The datasets supporting the conclusions of this article are included within the article and its additional supplementary file. The other raw and analysed datasets generated during the study are available for research purposes from the corresponding author on reasonable request.

Declarations

Ethics approval and consent to participate

Approvals were from the Methodist Research Institute's Institutional Animal Care and Use Committee.

Consent for publication

This manuscript has been read and approved by all authors, it has not been previously published, and is not under simultaneous consideration by another journal. Authors give consent for publication in *Molecular Neurodegeneration*.

Competing interests

The authors of this manuscript declare that they have no competing interests.

Author details

¹Stanley H. Appel Department of Neurology, Houston Methodist Research Institute, 6560 Fannin Street, Suite ST-802, Houston, TX 77030, USA. ²T. T. and W. F. Chao Center for BRAIN, Houston Methodist Hospital, Houston, TX, USA. ³Systems Medicine and Bioengineering Department, Houston Methodist Cancer Center, Houston, TX, USA.

Received: 12 September 2022 Accepted: 15 September 2022

Published online: 30 September 2022

References

- Schwartzentruber J, Cooper S, Liu JZ, Barrio-Hernandez I, Bello E, Kumasaka N et al (2021) Genome-wide meta-analysis, fine-mapping and integrative prioritization implicate new Alzheimer's disease risk genes. *Nat Genet* 53(3):392–402
- Jansen IE, Savage JE, Watanabe K, Bryois J, Williams DM, Steinberg S et al (2019) Genome-wide meta-analysis identifies new loci and functional pathways influencing Alzheimer's disease risk. *Nat Genet* 51(3):404–413
- McQuade A, Blurton-Jones M (2019) Microglia in Alzheimer's Disease: Exploring How Genetics and Phenotype Influence Risk. *J Mol Biol* 431(9):1805–1817
- Welikovitsh LA, Do Carmo S, Magloczky Z, Malcolm JC, Loke J, Klein WL et al (2020) Early intraneuronal amyloid triggers neuron-derived inflammatory signaling in APP transgenic rats and human brain. *Proc Natl Acad Sci U S A* 117(12):6844–6854
- Masliah E, Sisk A, Mallory M, Mucke L, Schenk D, Games D (1996) Comparison of neurodegenerative pathology in transgenic mice overexpressing V717F beta-amyloid precursor protein and Alzheimer's disease. *J Neurosci* 16(18):5795–5811
- Jung CK, Keppler K, Steinbach S, Blazquez-Llorca L, Herms J (2015) Fibrillar amyloid plaque formation precedes microglial activation. *PLoS ONE* 10(3):e0119768
- Venegas C, Kumar S, Franklin BS, Dierkes T, Brinkschulte R, Tejera D et al (2017) Microglia-derived ASC specks cross-seed amyloid-beta in Alzheimer's disease. *Nature* 552(7685):355–361
- Liu Y, Dai Y, Li Q, Chen C, Chen H, Song Y et al (2020) Beta-amyloid activates NLRP3 inflammasome via TLR4 in mouse microglia. *Neurosci Lett* 736:135279
- Nakanishi A, Kaneko N, Takeda H, Sawasaki T, Morikawa S, Zhou W et al (2018) Amyloid beta directly interacts with NLRP3 to initiate inflammasome activation: identification of an intrinsic NLRP3 ligand in a cell-free system. *Inflamm Regen* 38:27
- Lonnemann N, Hosseini S, Marchetti C, Skouras DB, Stefanoni D, D'Alessandro A et al (2020) The NLRP3 inflammasome inhibitor OLT1177 rescues cognitive impairment in a mouse model of Alzheimer's disease. *Proc Natl Acad Sci USA* 117(50):32145–32154
- Ising C, Venegas C, Zhang S, Scheiblich H, Schmidt SV, Vieira-Saecker A et al (2019) NLRP3 inflammasome activation drives tau pathology. *Nature* 575(7784):669–673
- Nilson AN, English KC, Gerson JE, Barton Whittle T, Nicolas Crain C, Xue J et al (2017) Tau oligomers associate with inflammation in the brain and retina of tauopathy mice and in neurodegenerative diseases. *J Alzheimers Dis* 55(3):1083–1099
- van Olst L, Verhaege D, Franssen M, Kamermans A, Roucourt B, Carmans S et al (2020) Microglial activation arises after aggregation of phosphorylated-tau in a neuron-specific P301S tauopathy mouse model. *Neurobiol Aging* 89:89–98
- Di J, Cohen LS, Corbo CP, Phillips GR, El Idrissi A, Alonso AD (2016) Abnormal tau induces cognitive impairment through two different mechanisms: synaptic dysfunction and neuronal loss. *Sci Rep* 6:20833
- Montagne A, Zhao Z, Zlokovic BV (2017) Alzheimer's disease: a matter of blood-brain barrier dysfunction? *J Exp Med* 214(11):3151–3169
- Montagne A, Nation DA, Sagare AP, Barisano G, Sweeney MD, Chakhoyan A et al (2020) APOE4 leads to blood-brain barrier dysfunction predicting cognitive decline. *Nature* 581(7806):71–76
- van de Haar HJ, Burgmans S, Jansen JF, van Osch MJ, van Buchem MA, Muller M et al (2017) Blood-brain barrier leakage in patients with early Alzheimer disease. *Radiology* 282(2):615
- Gate D, Saligrama N, Leventhal O, Yang AC, Unger MS, Middeldorp J et al (2020) Clonally expanded CD8 T cells patrol the cerebrospinal fluid in Alzheimer's disease. *Nature* 577(7790):399–404
- Xie L, Choudhury GR, Winters A, Yang SH, Jin K (2015) Cerebral regulatory T cells restrain microglia/macrophage-mediated inflammatory responses via IL-10. *Eur J Immunol* 45(1):180–191
- Rosenzweig N, Dvir-Szternfeld R, Tsitsou-Kampeli A, Keren-Shaul H, Ben-Yehuda H, Weill-Raynal P et al (2019) PD-1/PD-L1 checkpoint blockade harnesses monocyte-derived macrophages to combat cognitive impairment in a tauopathy mouse model. *Nat Commun* 10(1):465
- Kramer TJ, Hack N, Bruhl TJ, Menzel L, Hummel R, Griemert EV et al (2019) Depletion of regulatory T cells increases T cell brain infiltration, reactive

- astrogliosis, and interferon-gamma gene expression in acute experimental traumatic brain injury. *J Neuroinflammation* 16(1):163
22. Faridar A, Thome AD, Zhao W, Thonhoff JR, Beers DR, Pascual B et al (2020) Restoring regulatory T-cell dysfunction in Alzheimer's disease through ex vivo expansion. *Brain Commun*. 2(2):fcaa112
 23. Thonhoff JR, Beers DR, Zhao W, Pleitez M, Simpson EP, Berry JD et al (2018) Expanded autologous regulatory T-lymphocyte infusions in ALS: A phase I, first-in-human study. *Neurol Neuroimmunol Neuroinflamm* 5(4):e465
 24. Landel V, Baranger K, Virard I, Loriod B, Khrestchatskiy M, Rivera S et al (2014) Temporal gene profiling of the 5XFAD transgenic mouse model highlights the importance of microglial activation in Alzheimer's disease. *Mol Neurodegener* 9:33
 25. Oblak AL, Lin PB, Kotredes KP, Pandey RS, Garceau D, Williams HM et al (2021) Comprehensive evaluation of the 5XFAD mouse model for preclinical testing applications: a MODEL-AD study. *Front Aging Neurosci* 13:713726
 26. Wu DC, Hester J, Nadig SN, Zhang W, Trzonkowski P, Gray D et al (2013) Ex vivo expanded human regulatory T cells can prolong survival of a human islet allograft in a humanized mouse model. *Transplantation* 96(8):707–716
 27. Allen TM, Brehm MA, Bridges S, Ferguson S, Kumar P, Mirochnitchenko O et al (2019) Humanized immune system mouse models: progress, challenges and opportunities. *Nat Immunol* 20(7):770–774
 28. Bertilaccio MT, Scielzo C, Simonetti G, Ponzoni M, Apollonio B, Fazi C et al (2010) A novel Rag2-/-gammac-/-xenograft model of human CLL. *Blood* 115(8):1605–1609
 29. Lee K, Kwon DN, Ezashi T, Choi YJ, Park C, Ericsson AC et al (2014) Engraftment of human iPS cells and allogeneic porcine cells into pigs with inactivated RAG2 and accompanying severe combined immunodeficiency. *Proc Natl Acad Sci USA* 111(20):7260–7265
 30. Mutis T, van Rijn RS, Simonetti ER, Aarts-Riemens T, Emmelot ME, van Bloois L et al (2006) Human regulatory T cells control xenogeneic graft-versus-host disease induced by autologous T cells in RAG2-/-gammac-/-immunodeficient mice. *Clin Cancer Res* 12(18):5520–5525
 31. Vahedi F, Nham T, Poznanski SM, Chew MV, Shenouda MM, Lee D et al (2017) Ex vivo expanded human NK cells survive and proliferate in humanized mice with autologous human immune cells. *Sci Rep* 7(1):12083
 32. Baek H, Ye M, Kang GH, Lee C, Lee G, Choi DB et al (2016) Neuroprotective effects of CD4+CD25+Foxp3+ regulatory T cells in a 3xTg-AD Alzheimer's disease model. *Oncotarget* 7(43):69347–69357
 33. Jacob J, Nadkarni S, Volpe A, Peng Q, Tung SL, Hannen RF et al (2021) Spatiotemporal in vivo tracking of polyclonal human regulatory T cells (Tregs) reveals a role for innate immune cells in Treg transplant recruitment. *Mol Ther Methods Clin Dev* 20:324–336
 34. Mao L, Li P, Zhu W, Cai W, Liu Z, Wang Y et al (2017) Regulatory T cells ameliorate tissue plasminogen activator-induced brain haemorrhage after stroke. *Brain* 140(7):1914–1931
 35. Charan J, Kantharia ND (2013) How to calculate sample size in animal studies? *J Pharmacol Pharmacother* 4(4):303–306
 36. Arifin WN, Zahiruddin WM (2017) Sample size calculation in animal studies using resource equation approach. *Malays J Med Sci* 24(5):101–105
 37. Dansokho C, Ait Ahmed D, Aid S, Toly-Ndour C, Chaigneau T, Calle V et al (2016) Regulatory T cells delay disease progression in Alzheimer-like pathology. *Brain* 139(Pt 4):1237–1251
 38. Alves S, Churlaud G, Audrain M, Michaelsen-Preusse K, Fol R, Souchet B et al (2017) Interleukin-2 improves amyloid pathology, synaptic failure and memory in Alzheimer's disease mice. *Brain* 140(3):826–842
 39. Baruch K, Rosenzweig N, Kertser A, Deczkowska A, Sharif AM, Spinrad A et al (2015) Breaking immune tolerance by targeting Foxp3(+) regulatory T cells mitigates Alzheimer's disease pathology. *Nat Commun* 6:7967
 40. Mishra A, Kim HJ, Shin AH, Thayer SA (2012) Synapse loss induced by interleukin-1beta requires pre- and post-synaptic mechanisms. *J Neuro-immune Pharmacol* 7(3):571–578
 41. Hong S, Beja-Glasser VF, Nfonoyim BM, Frouin A, Li S, Ramakrishnan S et al (2016) Complement and microglia mediate early synapse loss in Alzheimer mouse models. *Science* 352(6286):712–716
 42. Leng F, Edison P (2021) Neuroinflammation and microglial activation in Alzheimer disease: Where do we go from here? *Nat Rev Neurol* 17(3):157–172
 43. Marsh SE, Abud EM, Lakatos A, Karimzadeh A, Yeung ST, Davtayan H et al (2016) The adaptive immune system restrains Alzheimer's disease pathogenesis by modulating microglial function. *Proc Natl Acad Sci USA* 113(9):E1316–E1325
 44. Spani C, Suter T, Derungs R, Ferretti MT, Welt T, Wirth F et al (2015) Reduced beta-amyloid pathology in an APP transgenic mouse model of Alzheimer's disease lacking functional B and T cells. *Acta Neuropathol Commun* 3:71
 45. McQuade A, Kang YJ, Hasselmann J, Jairaman A, Sotelo A, Coburn M et al (2020) Gene expression and functional deficits underlie TREM2-knockout microglia responses in human models of Alzheimer's disease. *Nat Commun* 11(1):5370
 46. Claes C, Danhash EP, Hasselmann J, Chadarevian JP, Shabestari SK, England WE et al (2021) Plaque-associated human microglia accumulate lipid droplets in a chimeric model of Alzheimer's disease. *Mol Neurodegener* 16(1):50
 47. Espuny-Camacho I, Arranz AM, Fiers M, Snellinx A, Ando K, Munck S et al (2017) Hallmarks of Alzheimer's disease in stem-cell-derived human neurons transplanted into mouse brain. *Neuron* 93(5):1066–1081
 48. Zhang H, Xia Y, Ye Q, Yu F, Zhu W, Li P et al (2018) In vivo expansion of regulatory T cells with IL-2/IL-2 antibody complex protects against transient ischemic stroke. *J Neurosci* 38(47):10168–10179
 49. Shi L, Sun Z, Su W, Xu F, Xie D, Zhang Q et al (2021) Treg cell-derived osteopontin promotes microglia-mediated white matter repair after ischemic stroke. *Immunity* 54(7):1527–1542
 50. Spangenberg E, Severson PL, Hohsfield LA, Crapser J, Zhang J, Burton EA et al (2019) Sustained microglial depletion with CSF1R inhibitor impairs parenchymal plaque development in an Alzheimer's disease model. *Nat Commun* 10(1):3758
 51. Baik SH, Kang S, Son SM, Mook-Jung I (2016) Microglia contributes to plaque growth by cell death due to uptake of amyloid beta in the brain of Alzheimer's disease mouse model. *Glia* 64(12):2274–2290
 52. Leyns CEG, Ulrich JD, Finn MB, Stewart FR, Koscal LJ, Remolina Serrano J et al (2017) TREM2 deficiency attenuates neuroinflammation and protects against neurodegeneration in a mouse model of tauopathy. *Proc Natl Acad Sci U S A* 114(43):11524–11529
 53. Dani M, Wood M, Mizoguchi R, Fan Z, Walker Z, Morgan R et al (2018) Microglial activation correlates in vivo with both tau and amyloid in Alzheimer's disease. *Brain* 141(9):2740–2754
 54. Sofroniew MV, Vinters HV (2010) Astrocytes: biology and pathology. *Acta Neuropathol* 119(1):7–35
 55. Frost GR, Li YM (2017) The role of astrocytes in amyloid production and Alzheimer's disease. *Open Biol* 7(12):1
 56. Habib N, McCabe C, Medina S, Varshavsky M, Kitsberg D, Dvir-Szternfeld R et al (2020) Disease-associated astrocytes in Alzheimer's disease and aging. *Nat Neurosci* 23(6):701–706
 57. Blasko I, Veerhuis R, Stampfer-Kountchev M, Saurwein-Teissl M, Eikelenboom P, Grubeck-Loebenstain B (2000) Costimulatory effects of interferon-gamma and interleukin-1beta or tumor necrosis factor alpha on the synthesis of Abeta1–40 and Abeta1–42 by human astrocytes. *Neurobiol Dis* 7(6 Pt B):682–689
 58. Hou L, Liu Y, Wang X, Ma H, He J, Zhang Y et al (2011) The effects of amyloid-beta42 oligomer on the proliferation and activation of astrocytes in vitro. *In Vitro Cell Dev Biol Anim* 47(8):573–580
 59. Ito M, Komai K, Mise-Omata S, Iizuka-Koga M, Noguchi Y, Kondo T et al (2019) Brain regulatory T cells suppress astrogliosis and potentiate neurological recovery. *Nature* 565(7738):246–250
 60. Rodriguez-Gomez JA, Kavanagh E, Engskog-Vlachos P, Engskog MKR, Herrera AJ, Espinosa-Oliva AM et al (2020) Microglia: agents of the CNS Pro-inflammatory Response. *Cells* 9(7):1

Publisher's Note

Springer Nature remains neutral with regard to jurisdictional claims in published maps and institutional affiliations.